Proceedings of the ASME 2010 3rd Joint US-European Fluids Engineering Summer Meeting and 8th International Conference on Nanochannels, Microchannels, and Minichannels
FEDSM-ICNMM2010
August 1-5, 2010, Montreal, Canada

FEDSM-ICNMM2010-30272

AEROACOUSTIC SOURCE DISTRIBUTION AROUND FOUR CYLINDERS ORIENTATED IN A SQUARE

Shane Leslie Finnegan*
Craig Meskell
Department of Mechanical and Manufacturing Engineering
Trinity College Dublin
Ireland
Email: finnegsl@tcd.ie

Peter Oshkai
Department of Mechanical Engineering
University of Victoria
Victoria, British Columbia
Canada

ABSTRACT

An experimental investigation of the flow-acoustic coupling of four cylinders arranged in a square configuration with a spacing ratio in the proximity interference range subject to forced acoustic resonance is presented. The aeroacoustic characteristics and the flow field structures are investigated at various sound pressure levels to study its influence on the "lock-in" behaviour of the separated flow and the corresponding distribution of the resonant acoustic sources. Two mainstream flow velocities were selected for testing that corresponded to flow field conditions before acoustic-Strouhal coincidence of the vortex shedding frequency with the natural acoustic frequency of the duct and to flow field conditions after acoustic-Strouhal coincidence. Increasing the sound pressure level was found to slightly increase the range of flow velocities with which the acoustics could entrain the vortex shedding regime. Increasing the sound pressure level was also found to shorten the length of the most intense vortical structures in the shear layers emanating from the upstream cylinders and hence also shifted the dominant acoustic sources upstream. Spatial distributions of the net acoustic energy suggests that the mechanism triggering acoustic resonance of the four cylinders is shear layer instability, which is similar to that observed for two tandem cylinders.

*Address all correspondence to this author.

INTRODUCTION

Flow-acoustic coupling is a phenomenon that can occur in various industrial engineering systems. Typical systems prone to flow-acoustic coupling are those that are found in a gas power plant and consist of ducted bluff bodies subject to cross flow, for example a heat exchanger. A heat exchanger generally has an array of tubes closely packed together in a duct subject to impinging flow normal to the axis of the tubes. Flow-acoustic coupling or acoustic resonance of such a system occurs when there is coupling/interaction between the shear layer oscillations (vortices) shed from the surface of the cylinders and the fluctuating acoustic modes of the ducts. Acoustic resonance induces a strong increase in the sound pressure fluctuations throughout the duct because of a feedback loop that establishes between the tubes and the duct walls and can be both annoying to plant personnel and a structural liability if it surpasses the dynamic head of the system.

As heat exchangers consist of numerous tubes orientated in an array, many investigations of the fluid mechanical and acoustic resonant characteristics of tubes bundles have been completed at both an experimental and industrial level. Various geometrical orientations of the tubes have been studied by Blevins and Bressler [1], Ziada et al. [2], Fitzpatrick [3], Parker [4] and Eisinger and Sullivan [5] to name a few. These studies have all given a comprehensive oversight into the physics of tube arrays and have also provided design rules and criteria for the particular geometries selected by the authors.

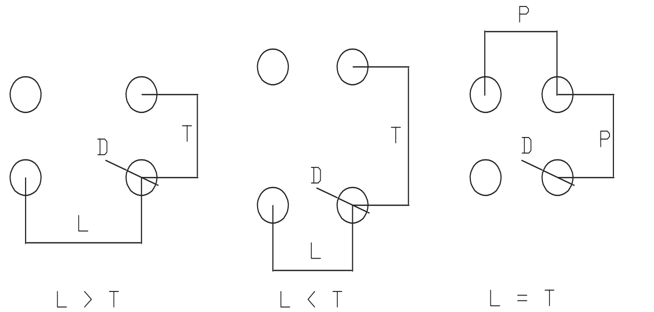

Figure 1. The three possible configurations of an in-line tube bundle.

One particular tube bundle orientation is the in-line geometry, which consists of four neighbouring cylinders positioned in such a way that they form either a square or rectangle, see Fig. 1. The important characteristic lengths of such an array are the spanwise centre to centre spacing ratio (L/D) and the streamwise centre to centre spacing ratio (T/D) where D is the diameter of the four cylinders. A full in-line array consists of many of these square/rectangular patterns clustered together. If $T/D = L/D$, the orientation is referred to as a square in-line array. In this case it is more convenient to classify the characteristic length as the centre to centre pitch ratio (P/D), see Fig. 1. Various authors have investigated the fluid mechanical characteristics of a two row, two column square in-line array (four cylinders orientated in a square) and whilst this arrangement may be less complex than a full in-line array, it still exhibits some of the characteristics of an in-line tube array.

Numerical simulation of the flow field characteristics around four cylinders orientated in a square have been completed by Lam et al [6] and Farrant et al. [7] for $1.6 \leq P/D \leq 5.0$ and for Reynolds numbers, $Re \leq 200$. They both found that the flow regime can exhibit either in-phase vortex shedding, anti-phase vortex shedding or synchronised vortex shedding between the cylinders. Flow visualisation by Lam et al. [6] agreed well with their own simulations and with those of Farrant et al. [7]. Lam and Lo [8] and Lam and Fang [9] have experimentally studied the flow field characteristics for similar configurations but at higher Reynolds numbers, $Re > 2000$. Their studies concentrated on the vortex shedding characteristics (pattern and Strouhal number) and the effect of the orientation of the cylinders with respect to the oncoming flow on the pressure distributions around the cylinders respectively.

These studies provided good insight into the flow structure around four cylinders orientated in a square, however, neglected the effect of acoustic resonance. Furthermore, there has been no attempt by anybody at an investigation of flow-acoustic coupling around a group of four cylinders orientated in a square. Such an investigation would reveal those areas in the flow which contribute positive net acoustic energy (sources) and those that contribute negative net acoustic energy (sinks) over an acoustic

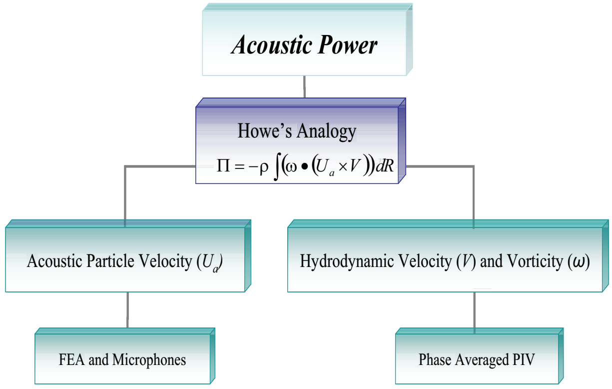

Figure 2. The conceptual approach used to investigate flow-acoustic coupling around the four cylinders in a square configuration.

wave cycle. If the source/sink locations could be located, engineers would be able to design appropriate mitigation techniques to subdue or even avoid acoustic resonance.

It is well known that acoustic resonance is driven by acoustic “lock-in”, which is a flow regime that occurs near the coincidence of the vortex shedding frequency with the natural acoustic frequency of the duct (acoustic-Strouhal coincidence). Here, the vortex shedding process from the cylinders becomes entrained to the duct's acoustic field. Finnegan et al. [10, 11] studied the flow-acoustic coupling mechanism of a “locked-in”' flow field around two tandem cylinders. The motivation for that investigation was to develop a spatial distribution of the resonant acoustic sources in a tube array. However, as they pointed out, significant challenges present themselves which make such an investigation very difficult to do experimentally and that geometric complexity of the tested array should be increased iteratively.

The motivation for this study, which presents an experimental investigation of the flow-acoustic coupling around four cylinders orientated in an in-line square formation subject to ducted flow and forced transverse acoustic resonance, is the same as Finnegan et al. [10, 11]. In fact, this work is a direct extension of their study and is the next iteration in geometric complexity for a bluff body system subject to cross flow. Identification of the location and nature of the acoustic sources is completed using the theoretical framework developed by Howe [12, 13], which is summarised in Fig. 2. As can be seen, a combination of finite element analysis, microphone measurements of the acoustic pressure and quantitative images of the flow field using particle image velocimetry (PIV) can be used to form an experimental model for the calculated acoustic power, Π.

EXPERIMENTAL SETUP AND TECHNIQUE

Tests were completed in an open loop draw down wind tunnel and utilised air as the working fluid. A schematic of the test section can be seen in Fig. 3 which had a span of 320mm and a main duct width of 125mm. The tested four cylinder configuration had a pitch ratio, $P/D = 2.5$, with a cylinder diameter, $D = 13$mm. The centre of the cylinder, labelled $C1$ in Fig. 3, was used as the origin of coordinate system for the current experiments. The orientation of the x-direction and $y$direction can also be seen in Fig. 3. The spacing ratio of the cylinders was within proximity interference region as defined by Zdravkovich [14] and was selected so that the "locked-in" flow structure and the distributions of the resonant acoustic sources could be compared to the two tandem cylinder case investigated by Finnegan et al [10, 11]. Two circular side-branches with diameter, $L_c = 125$mm and depth, $D_c = 220$mm, were attached to the walls of the test section because the maximum flow velocity in the tunnel, $V_\infty = 44$m/s, which was measured by pitot-static tube far upstream of the cylinders was insufficient to excite the first transverse acoustic mode of the duct when it had an entirely square cross section. Adding the side-branches lowered the natural acoustic frequency of the duct and thereby brought the acoustic "lock-in" range to the capability of the fan. The four cylinders were located in the middle of the test section where the acoustic particle velocity, (U_a) is maximum. Excitation of the lowest resonance mode was achieved by varying sound pressure level (SPL) amplitude in the duct by means of a loudspeaker attached to one end of the closed side-branches. SPL amplitudes of 155 dB and 158 dB when there was no flow in the duct were selected for testing. The input frequency of the loudspeaker corresponded to the first natural acoustic mode of the duct, $f_a = 329$Hz, which was measured using white-noise excitation without any flow across the cylinders. The loud-speaker was totally encased within a chamber made from industrial piping that mounted easily onto the test section at the end of the side-branches. The side of the chamber exposed to the duct during testing had holes drilled in a concentric circular pattern to maximise acoustic transparency whilst retaining a hard walled boundary condition. The chamber also had a small bleed line that led from the back of the chamber to a small tap inserted in the side branch in order to equalise the pressure on both sides of the loudspeaker cone.

Initially, measurements of the unsteady pressure fluctuations in the flow, as a function of mainstream flow velocity were taken using a flush mounted G.R.A.S Type 40BH microphone, M1 as shown in Fig.3. The pressure measurements of the flow were then used to determine the range of flow velocities for which the vortex shedding regime was entrained ("locked-in"') to the acoustic field and hence was also used to determine the flow velocities at which to complete quantitative PIV analysis of the flow field. It was desired that the selected flow velocities be "locked-in"' to the acoustic field for both SPL amplitudes. Mainstream velocities of $V_\infty = 20.76$m/s and $V_\infty = 25.37$m/s corresponded to this constraint. 100 PIV images of the unsteady flow field were acquired for every 22.5° of the acoustic pressure wave cycle which meant it was split into 16 different phases. A new

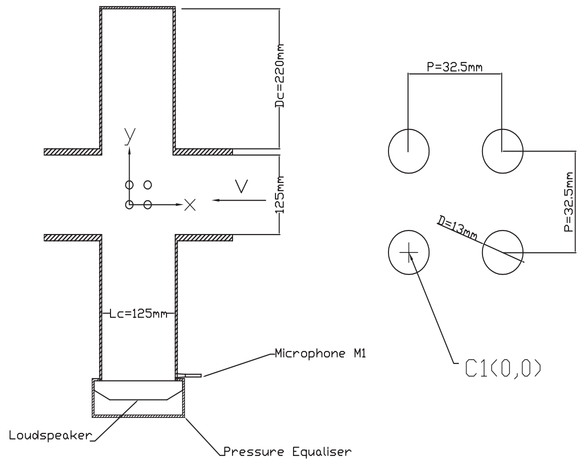

Figure 3. Schematic of the experimental test section.

PIV acquisition (i.e. 100 PIV recordings) was completed for each phase and the internal timing of the PIV Q-switch was altered in order to acquire the images at the various phases. The order in which the phases were recorded was randomised so that any unknown bias from the measurement was removed. Due to the high velocity gradients between the free-stream and the cylinder gap/wake regions, a multi-pass correlation algorithm that involved reducing the interrogation window size from $32px \times 32px \rightarrow 12px \times 12px$ with 50% overlap in both the x- and y-directions was used to calculate the velocity vectors from the pairs of images of the flow tracers. Further descriptions of the PIV experimental/processing characteristics can be found in Finnegan et al. [11].

RESULTS

Acoustics

The aeroacoustic characteristics of the four cylinders can be seen in Fig. 4 which shows a plot of the vortex shedding frequency measured by Microphone M1 as a function of the reduced velocity, which is defined as $Ur = V_\infty/(f_a D)$. As can be seen, for the case where there is no applied sound, the vortex shedding frequency increases linearly with velocity and does not exhibit self initiated "lock-in"'. The Strouhal number of vortex shedding based on mainstream velocity and the cylinder diameter was calculated as $St = 0.179$. This shows good agreement with values published in literature, particularly the numerical simulations of Farrant et al. [7] who reported $St = 0.177$. If sound is applied through the loud speakers, it is clear to see that the vortex shedding frequency becomes entrained or "locked-in"' to the acoustic forcing frequency at $U_r = 4.85$ for each SPL amplitude. The "lock-in"' phenomenon then continues for a range of reduced velocities, through acoustic-Strouhal coincidence and then subsides at $U_r = 6.2$ for the $SPL = 155$dB case and at $U_r = 6.44$ for

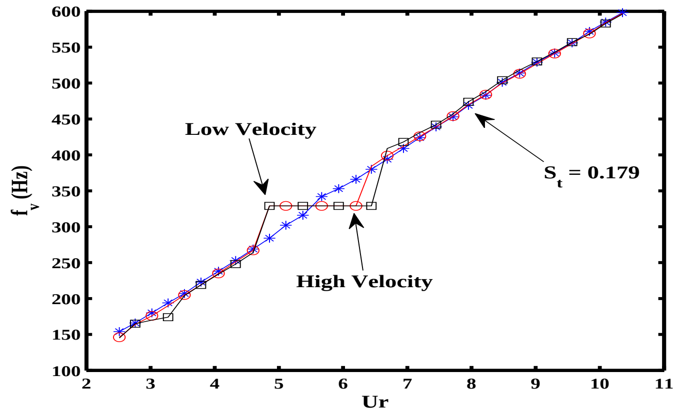

Figure 4. Aeroacoustic characteristics measured by microphone M1; □ $SPL = 158$dB, ○ $SPL = 155$dB, ∗ No applied sound.

V_∞ (m/s)	U_r	A (Pa)	$\overline{U}_a$	$\overline{U}_a/V_\infty$
20.76	4.85	700	1.63	0.078
20.76	4.85	1044	2.43	0.117
25.37	5.93	242	0.57	0.022
25.37	5.93	1152	2.67	0.105

Table 1. Summary of the experimental parameters.

the $SPL = 158$dB case.

The behaviour shown in Fig. 4 is similar to that reported for two tandem cylinders by Finnegan et al. [10, 11] and Mohany and Ziada [15] who classified two acoustic resonance ranges, namely pre-coincidence resonance which occurs before acoustic-Strouhal coincidence and coincidence resonance which occurs after. Oengoren and Ziada [16] also observed a similar phenomenon for a full in-line tube array. As mentioned above, the pressure measurements from M1 were used to determine the flow velocities at which to perform quantitative PIV measurements. These are also shown on Fig 4 and are labelled as "Low velocity"' and "High velocity"'. The Low velocity case corresponds to a reduced velocity $U_r = 4.85$ whilst the high velocity case corresponds $U_r = 5.93$. Based on the measured Strouhal number, acoustic-Strouhal coincidence occurs at $U_r = 5.58$. Therefore, the ratio between the acoustic forcing frequency and the natural vortex shedding frequency is $f_a/f_v = 1.15$ for the low velocity case and $f_a/f_v = 0.94$ for the high velocity case.

The finite element package ANSYS was used to perform modal analysis of a quiescent flow field in the test section and to solve the resonant acoustic pressure distribution (i.e. mode shape) with the cylinders present. Equation 1 was used to solve the time dependent acoustic particle velocity in the test section. This equation is an expanded version of the Euler equation where P_{rms} denotes the root mean square of the amplitude of the time trace of microphone $M1$, P_{FEA} denotes the pressure solved from the modal analysis and $\rho = 1.25\text{kg/m}^3$ represents the mean density of air. Assuming planar acoustic wave propagation in the test section, the nominal acoustic particle velocity amplitude, $\overline{U}_a$ can be estimated from Eqn. 2 where $c = 343$m/s is speed of sound in air. From this, the dimensionless acoustic particle velocity can be obtained as the ratio between the acoustic particle velocity amplitude and the mainstream duct velocity ($\overline{U}_a/V_\infty$). This is an indication of the forcing applied by the loudspeaker. Table 1 summarises the dimensionless acoustic particle velocities of the tested cases. For each case, the dimensionless acoustic particle velocity was calculated using the pressure value measured by M1.

Figure 5 shows the profile along the centreline of the side-branches of the lowest resonant acoustic mode shape calculated in the duct and the shape of the acoustic particle velocity, calculated using Eqn. 1. As can be seen, one half of a wavelength is completed across both side-branches which means that an acoustic pressure node exists between the cylinders, which also means that the acoustic particle velocity is maximum between the cylinders. A slight asymmetry can be seen in the pressure and acoustic particle velocity distributions in Fig 5. This occurred because the pressure normalisation chamber added 20mm to the side-branch which meant there was a slight geometric asymmetry in the test section. This geometric discrepancy was accounted for in the model and explains the asymmetry in the mode shape. The frequency of the acoustic particle velocity solved by the model was 304Hz. The natural frequency measured by M1 on the day of testing was 329Hz, which is 8.2% higher than the numerically computed value. This variation has been attributed to the presence of the loudspeaker at the closed end of the side-branch, which was not modelled as the walls where assumed to be an ideal rigid acoustic medium. The boundary conditions applied to the model were zero acoustic pressure at the inlet and outlet of the test section, making it a Dirichlet boundary-value problem [17]. This boundary condition was selected in order to simulate an open ended duct which facilitated the extraction of the β-mode [18], where the pressure decays exponentially along the length of the duct.

$$U_a(x,y,t) = \frac{A}{2\pi f_a \rho} cos(2\pi f_a t) \cdot \nabla P_{FEA} \tag{1}$$

$$\overline{U}_a = \frac{P_{rms}}{c\rho} \tag{2}$$

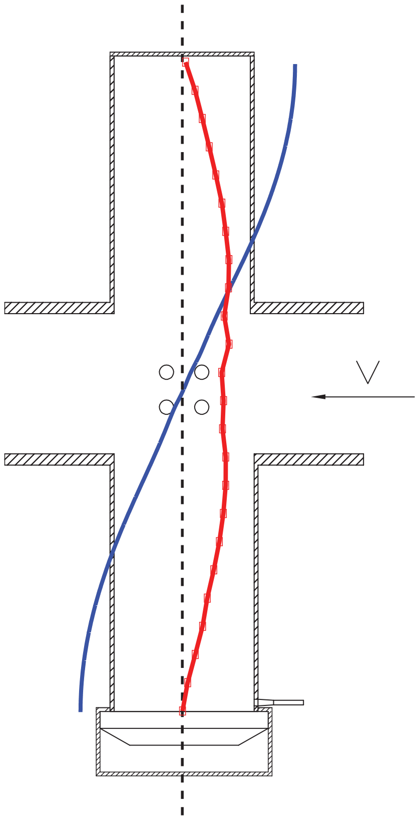

Figure 5. Distributions of the resonant acoustic mode shape in the test section. — Acoustic pressure pressure, □ acoustic particle velocity.

Phase Averaged Flow Structure

Howe [12] reformulated the Lighthill's [19] aerodynamic theory of sound to include the effect of a non uniform mean flow on the generation of sound and deduced that the acoustic sources in the flow solely correspond to regions where the vorticity is non-vanishing. Quantitative visualisation of the resonant flow field structures identifies those regions of the flow where vorticity is non vanishing. Figure 6 shows contour plots of the out of plane vorticity in the flow field around the cylinders for four different phases of the acoustic cycle and shows the evolution of the vortical structures as they propagate downstream. The phases shown here, $\phi = 22.5°$, $112.5°$, $202.5°$ and $292.5°$, refer to the phase to the acoustic pressure wave measured by M1. These images describe the flow field structures when $f_a/f_v = 1.15$ and $\overline{U}_a/V_\infty = 0.117$. They are the averages of the 100 PIV recordings taken at the respective phases. Contours of positive vorticity are coloured red with black trim whilst contours of negative vorticity are coloured blue with green trim. Also shown on the plots is an image of the four cylinders in the PIV image plane. As can be seen, there are regions of the flow where velocity vectors could not be resolved due the presence of the cylinders. Shadowing behind the cylinders, reflections from the cylinders (due to impingement of the laser sheet with cylinders) and parallax along the surface of the cylinders all prevented velocity vectors from being calculated in these regions.

Consider the four cylinders to be equivalent to two pairs of two tandem cylinders. At $\phi = 22.5°$, a vortex is shed from the bottom side of both upstream cylinders which then rolls up in the gap region between $\phi = 112.5°$ and $\phi = 202.5°$ and finally impinges on the downstream cylinder at $\phi = 292.5°$. After the vortex impinges on the downstream cylinders it triggers another vortex in the wake. The same behaviour occurs for vortices shed from the top side of either upstream cylinder and so two Von-Karman vortex streets form in the wake of the four cylinders, one for each pair of tandem cylinders.

This type of vortex shedding regime can be described as anti-symmetric, that is the location and development of vortices shed from the same side of the upstream cylinders match. Furthermore, it can also be seen that the vortices shed between the upstream and downstream cylinders are in phase with each other. This "locked-in"' flow structure closely resembles the flow structure reported by Finnegan et al [10, 11] for two tandem cylinders with the same pitch ratio and it should be noted that a similar pattern was also observed for the other tested cases ($\overline{U}_a/V_\infty = 0.078, 0.022, 0.105$). It can also be seen from Fig. 6 that vortices shed from either pair of tandem cylinders do not interact with the other pair of cylinders nor do they interact with the vortices shed from that pair. This must be due to the spacing ratio of current orientation, $P/D = 2.5$. An investigation into the critical spacing ratio where interaction occurs could be interesting.

Phase Averaged Acoustic Power

A simple expression developed by Howe [12,13] for the dissipation of sound from an edge can be used to couple the unsteady vorticity in the shear layers around the cylinders with the variation of the velocity across the duct and the fluctuating transverse acoustic wave imposed by the loudspeakers. This equation, Eqn. 3 calculates the instantaneous acoustic power generated by the cylinders in the flow. Howe's integral can be expressed as

$$\Pi = -\rho \int \underline{\omega} \cdot (\underline{U_a} \times \underline{V}) d\Re \tag{3}$$

and is the volume integral of the triple product between the vorticity vector $\underline{\omega}$, the flow velocity vector $\underline{V}$ and the acoustic particle velocity vector $\underline{U_a}$ where ρ is the mean density of the fluid in the volume $\Re$. The net acoustic energy is calculated by integrating the acoustic power generated at each phase over the whole

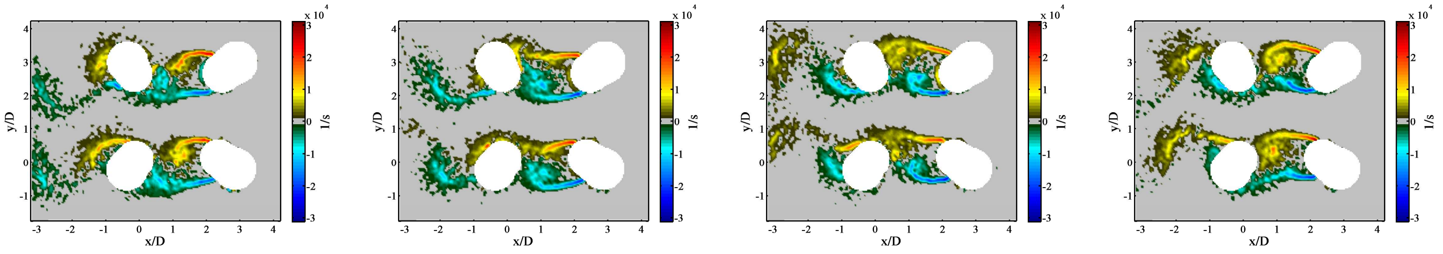

$\phi = 292.5°$ $\phi = 202.5°$ $\phi = 112.5°$ $\phi = 22.5°$

Figure 6. Contours of the "locked-in" out of plane vorticity around the cylinders. $f_a/f_v = 1.15$, $\overline{U}_a/V_\infty = 0.117$.

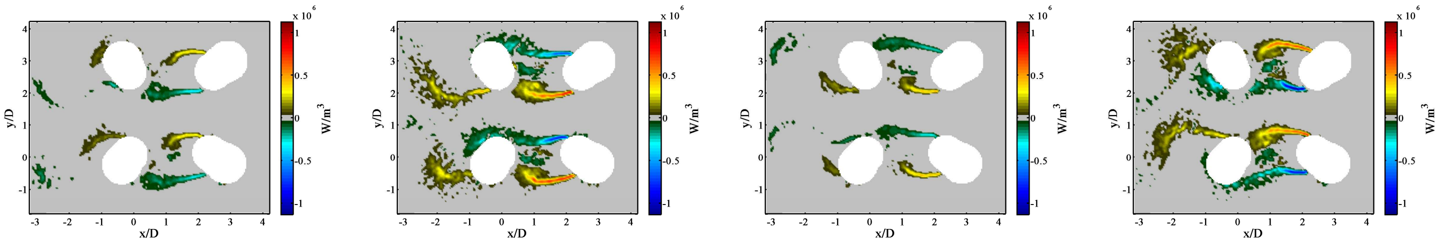

$\phi = 292.5°$ $\phi = 202.5°$ $\phi = 112.5°$ $\phi = 22.5°$

Figure 7. Contours of the acoustic power around the cylinders, highlighting the distribution of the acoustic sources and sinks at different phases of the acoustic pressure wave cycle. $f_a/f_v = 1.15$, $\overline{U}_a/V_\infty = 0.117$.

acoustic wave cycle, that is integrating the acoustic power over all the 16 phases of acoustic pressure wave. Acoustic energy will be generated if the integral is positive over the whole cycle and absorbed if the integral is negative over the whole cycle. Various authors have utilised Eqn. 3 to analyse flow-acoustic coupling for a range of different engineering applications from Hourigan et al. [17] for acoustic resonance in a duct with baffles to Velikorodny et al. [20] for a co-axial side-branch resonator.

Figure 7 plots the acoustic power calculated by the integrand of Eqn. 3 when $f_a/f_v = 1.15$ and $\overline{U}_a/V_\infty = 0.117$ at $\phi = 22.5°, 112.5°, 202.5°, 292.5°$ in the acoustic pressure wave cycle. The images in the first and third columns from the right ($\phi = 22.5°$ and $202.5°$) correspond to phases where the acoustic particle velocity has just passed through its maximum positive and maximum negative amplitude respectively. As the acoustic particle velocity magnitude is still high at these phases, a large amount of acoustic power is generated (and absorbed) as can be seen from the scales. The images in the second and fourth columns from the right ($\phi = 112.5°$ and $\phi = 292.5°$) correspond to phases where the acoustic particle velocity has just passed through zero. As the acoustic particle velocity magnitude is still low at these phases, a relatively small amount of acoustic power is generated (and absorbed) when compared to $\phi = 22.5°$ and $202.5°$. It is clear that the distribution of acoustic power resembles the distribution of vorticity for each phase. At $\phi = 22.5°$, the positive vortices shed from the top sides the cylinders are generating acoustic power whilst the negative vortices shed from the bottom side are all absorbing power. The opposite can be said at $\phi = 202.5°$ as the positive vortices (shed from the top of the cylinder) are absorbing acoustic power whilst the negative vortices (shed from the bottom of the cylinders) are generating acoustic power. That is to say, the acoustic sources have changed polarity. This is due to the simple fact that the acoustic particle velocity changes sign as it passes through zero at $\phi = 90°$ and $\phi = 270°$.

Time Averaged Flow Structure

The time averaged out of plane vorticity structures of the flow field around the four cylinders can be seen in Fig. 8 for all the tested cases. The figure highlights the locations of the most intense vortex structures in the flow and shows the development of the shear layer thickness over a whole acoustic cycle. As can be seen, for each tested velocity, a thin shear layer sheds from the upstream cylinders and thickens as it propagates downstream. It can also be seen the most intense vortex structures (both polarities) are located at the separation points on the upstream cylinder and that the intensity of the shear layer reduces as travels downstream. The intensity of the vortices shed into the wake, downstream of the cylinders is much lower and also far less defined when compared to the structures propagating in the

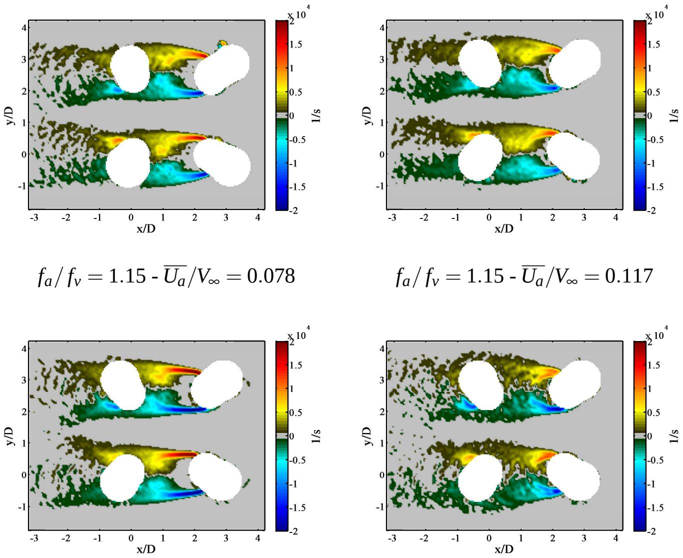

$f_a/f_v = 1.15$ - $\overline{U_a}/V_\infty = 0.078$ $f_a/f_v = 1.15$ - $\overline{U_a}/V_\infty = 0.117$

$f_a/f_v = 0.94$ - $\overline{U_a}/V_\infty = 0.022$ $f_a/f_v = 0.94$ - $\overline{U_a}/V_\infty = 0.105$

Figure 8. Contours of the time averaged out of plane vorticity.

shear layer gap region. Furthermore, increasing the dimensionless acoustic velocity, $\overline{U}_a/V_\infty$, seems to shift the location of the most intense structures in the shear layer upstream and reduce their corresponding intensity. This means that the shear layers in the gap region between the cylinders become more unsteady as the sound pressure level increases.

Time Averaged Acoustic Power - Net Acoustic Energy

The net acoustic energy generated over the whole cycle can be found by integrating Eqn. 3. Figure 9 shows the spatial distributions of the net acoustic energy for all the tested cases. As can be seen, the structure of the aeroacoustic sources surrounding one tandem cylinder pair are very similar to those surrounding the other tandem cylinder pair for each of the tested cases. In fact, the aeroacoustic sources generated between the two pairs of tandem cylinders are mirror images of each other. For example, the gap region between the top pair of tandem cylinders for $f_a/f_v = 1.15$ and $\overline{U_a}/V_\infty = 0.078$ exhibits two equal length sources hugged by two odd length sinks. The sink hugging the source on the top shear layer is the longer than the sink hugging the source on the bottom shear layer. If the bottom pair of tandem cylinders is now inspected, one can see the same effect except now the bottom sink is the longer of the two sinks hugging the sources. If one looks closer again, it can be seen that all four sources in the shear layer gap region are hugging sinks, the longest and most intense being shed from the bottom side of the upstream cylinder in the top tandem cylinder pair and from the top side of the upstream cylinder on the bottom tandem cylinder pair. This mirror imaging behaviour of the aeroacoustic sources

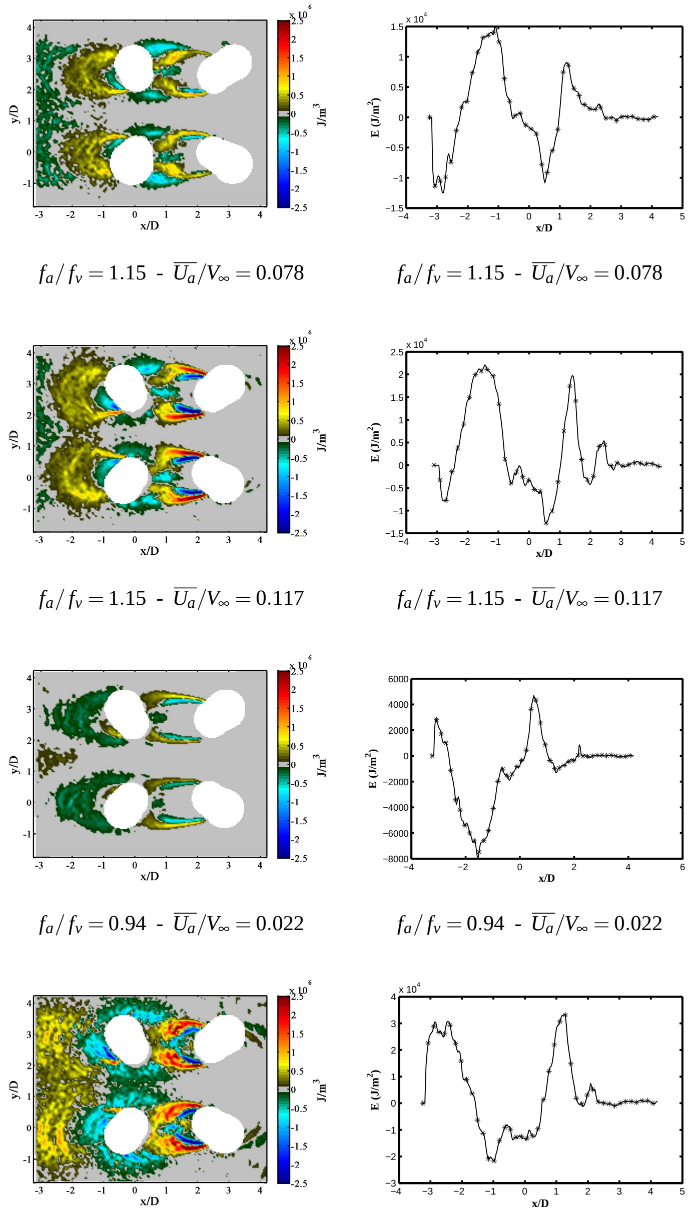

$f_a/f_v = 1.15$ - $\overline{U_a}/V_\infty = 0.078$ $f_a/f_v = 1.15$ - $\overline{U_a}/V_\infty = 0.078$

$f_a/f_v = 1.15$ - $\overline{U_a}/V_\infty = 0.117$ $f_a/f_v = 1.15$ - $\overline{U_a}/V_\infty = 0.117$

$f_a/f_v = 0.94$ - $\overline{U_a}/V_\infty = 0.022$ $f_a/f_v = 0.94$ - $\overline{U_a}/V_\infty = 0.022$

$f_a/f_v = 0.94$ - $\overline{U_a}/V_\infty = 0.105$ $f_a/f_v = 0.94$ - $\overline{U_a}/V_\infty = 0.105$

Figure 9. Contours of the resonant net acoustic energy for all the tested cases.

can also be observed for the other tested cases apart from the $f_a/f_v = 0.94$ and $\overline{U_a}/V_\infty = 0.105$ case where the distribution of sources between the cylinder pairs seems to be symmetric.

DISCUSSION

Regions of the unsteady hydrodynamic flow field characteristics have been successfully coupled with the fluctuating acoustic particle velocity around four cylinders orientated in a square. Spatial distributions of the net acoustic energy generated by the flow across the cylinders over the entire acoustic wave cycle have been produced. Apart from spatial distributions of the net acoustic energy, Fig. 9 also shows the net acoustic energy transfer per spanwise location which indicates where the main acoustic sources and sinks are located in the normalised x-direction, x/D. As can be seen a net source in the gap region between the cylinders exists for all of the cases. It can also be seen by comparing the spatial distributions of the sources with the net acoustic energy transfer that the regions surrounding the downstream cylinders are mainly acoustic sinks and so, the total net energy transfer is negative. This means that as the vortices impinge on the downstream cylinder, they transfer energy from the acoustic field to the hydrodynamic flow field which is balanced by radiation and viscous damping. In the wake region for the $f_a/f_v = 1.15$ case, strong net sources exist between $-1 \leq x/D \leq 2.5$. The wake appears to contribute more to the acoustic resonance than the gap region as the magnitude and broadness of the peak source is larger than the peak source in the gap region. However, because the field of view was limited to the region around the cylinders it is difficult to say how the wake far downstream of the cylinders will contribute. It does seem though that energy will be generated and absorbed in a periodic fashion in the wake. For the $f_a/f_v = 0.94$ case, acoustic sinks formulate in the immediate region downstream of the cylinders. Increasing the dimensionless acoustic velocity, from $\overline{U_a}/V_\infty = 0.022$ to $\overline{U_a}/V_\infty = 0.105$ seems to shorten the length of the sink regions whilst promoting source regions

The excitation of the four cylinders are analogous to the fluid-dynamic oscillations of a simple cavity detailed by Rockwell and Naudascher [21] where the primary mechanism of the oscillations are the amplification of the vortices in the shear layer and a feedback which establishes because of the presence of the downstream cavity edge. As a distinct source exists in the gap region between the cylinders that is sustaining resonance, feedback (or the upstream propagation) of the vortical disturbances must occur. It must also produce extra vortices at the separation point on the upstream cylinders which would be amplified in the shear layer. The sources and sinks in the wake seem to be generated by large scale vortices propagating alternatively in a Von Karman vortex street. The polarity of the acoustic energy generated depends on the polarity of the vortex located in a the region at a particular phase.

The Influence of SPL on the Aeroacoustic Sources

Varying the SPL simply acts as a scaling factor in Eqn. 3 because the acoustic particle velocity is proportional to the SPL. In order to properly observe the effect of the SPL amplitude, it should be taken out of consideration. A dimensional analysis of the system, revealed that the energy per spanwise location, E

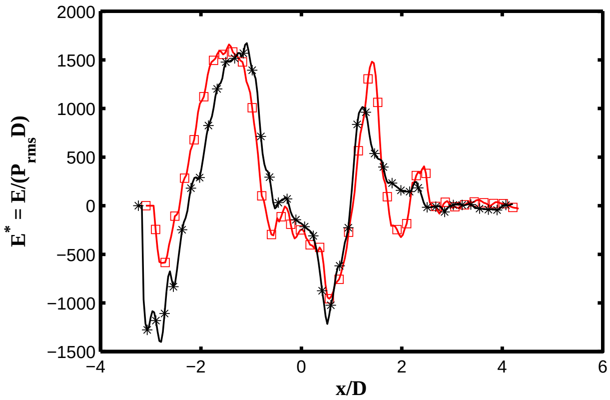

Figure 10. Normalised net acoustic energy transfer per spanwise (E^*), $f_a/f_v = 1.15$ ($U_r = 4.85$); $*$ $\overline{U_a}/V_\infty = 0.078$, $\square$ $\overline{U_a}/V_\infty = 0.117$.

(J/m^2), can be normalised by the product of acoustic pressure measured by microphone M1 during a test and the cylinder diameter, that is,

$$E^* = \frac{E}{P_{rms}D} \tag{4}$$

Figure. 10 and Fig. 11 plot the normalised energy transfer per spanwise location, E^*, calculated using Eqn. 4, for the $f_a/f_v = 1.15$ and $f_a/f_v = 0.94$ cases respectively. The figures compare the $\overline{U_a}/V_\infty$ at each flow velocity and give a good indication of the influence that the SPL has on the vortex-induced aeroacoustic sources. For the $f_a/f_v = 1.15$ case, increasing the SPL does not appreciably effect the strength of the sources in the wake of the four cylinders nor does it appreciably effect their distribution. However, the same can not be said for the source in the gap region as increasing $\overline{U_a}/V_\infty = 0.078$ to $\overline{U_a}/V_\infty = 0.117$ considerably increases the strength of the source and shifts it towards the upstream cylinders. This is in line with the observation made from Fig. 8.

A similar behaviour is exhibited for the $f_a/f_v = 0.94$ case as an increase in the source's strength occurs which is accompanied by a significant shift towards the upstream cylinder. This shift is more pronounced than observed for the $f_a/f_v = 1.15$ case. The wake of the $f_a/f_v = 0.94$ case appears to show more sensitivity to changes in the SPL compared to the $f_a/f_v = 1.15$ case. As can be seen, the location of the peak sources and sinks shift upstream with increasing SPL. Furthermore, the magnitude of these peak sources increase whilst the magnitude of the sinks decrease with increasing SPL. The trends observed in Fig. 10 and Fig. 11 seem to support the observations made from the spatial distributions of energy, Fig. 9.

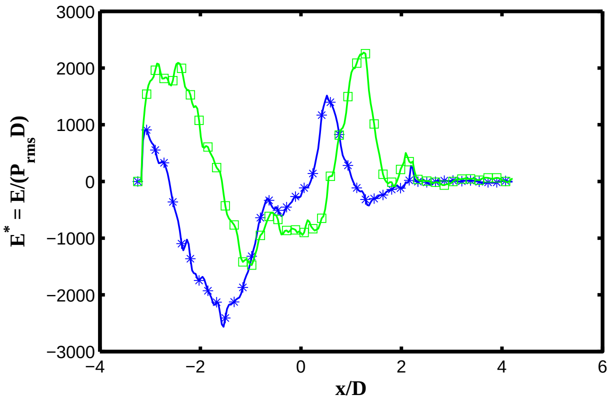

Figure 11. Normalised net acoustic energy transfer per spanwise (E^*), $f_a/f_v = 0.94$ ($U_r = 5.93$); $*$ $\overline{U_a}/V_\infty = 0.022$, $\square$ $\overline{U_a}/V_\infty = 0.105$.

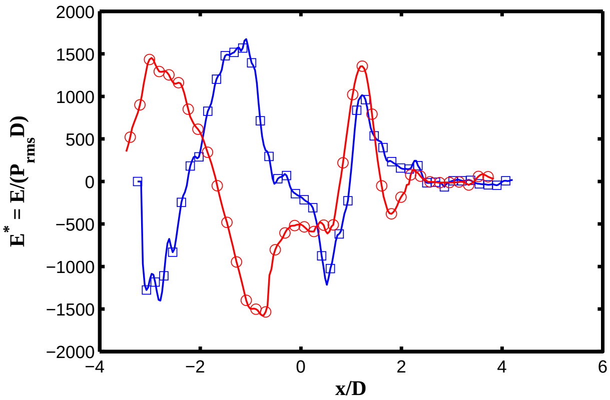

Figure 12. Normalised net acoustic energy transfer per spanwise (E^*). $\square$ Four Cylinders ($f_a/f_v = 1.15$ $\overline{U_a}/V_\infty = 0.078$), $\circ$ Two Tandem Cylinders ($f_a/f_v = 1.12$ $\overline{U_a}/V_\infty = 0.07$) [22].

Comparison with Two Tandem Cylinders

Figure 4 highlights the range of flow velocities with which the vortex shedding regime becomes entrained to the acoustic field for the four cylinders. As can be seen, the flow field becomes “locked-in”’ to the acoustic field before acoustic-Strouhal coincidence, which is similar to that observed by Finnegan et al. [22] for two tandem cylinders subject forced acoustic resonance. Figure 12 compares the normalised net acoustic energy transfer of four cylinders with $f_a/f_v = 1.15$ and $\overline{U_a}/V_\infty = 0.117$ against that observed by Finnegan et al. [22] for two tandem cylinders with a similar set of experimental parameters. As can be seen for both the four cylinder and two tandem cylinder cases, strong sources exist in the gap region at roughly $x/D = 1.5$ whilst transfer of acoustic energy from the sound field to the flow field occurs at the downstream cylinders. In the wake region, the strength of the sources seem to be comparable. However, it can be seen that the peak source of the four cylinder arrangement occurs in the same spanwise location as the peak sink of the tandem cylinders whilst the peak sink of the four cylinders occurs in the same spanwise location as the peak source of the two tandem cylinder. That is to say, the sources in the wake region are out of phase with each other. Finnegan et al. [11] reported that the aeroacoustic sources in the wake of the tandem cylinders generate and absorb energy periodically and inspection of Fig. 12 suggests that this will also occur for the four cylinder case as well. Mohany and Ziada [15, 23] suggested that the pre-coincidence resonance mechanism for two tandem cylinders was triggered by instability in the gap shear layer. Finnegan et al. [10, 11] supported this and further proposed that the vortex shedding in the wake might also contribute to pre-coincidence acoustic resonance. This also seems to be the case for a set of four cylinders orientated in a square looking at the current data and remembering that should generate and absorb acoustic energy periodically.

CONCLUSIONS

A semi-empirical investigation of the flow-acoustic coupling of four tandem cylinders with a spacing ratio in the proximity interference range subject to forced transverse acoustic resonance has been presented. The aeroacoustic characteristics and the flow field structures were investigated at various sound pressure levels to study its influence on the “lock-in”’ behaviour of the cylinders and the corresponding distribution of the resonant acoustic sources. Two mainstream flow velocities were selected for testing, one before acoustic-Strouhal coincidence and once after acoustic-Strouhal coincidence. The separated flow became “locked-in”’ with the acoustics of the duct before acoustic-Strouhal coincidence which is similar to that reported in literature for two tandem cylinders. Moreover, acoustic “lock-in”’ was found to exist after acoustic-Strouhal coincidence and could be extended by increasing the sound pressure level in the duct. Increasing the sound pressure level did not have the same effect on the “lock-in”’ range before acoustic-Strouhal coincidence. Investigation of the time averaged vorticity suggested that increasing the sound pressure level shortens the length of the most intense vortical structures in the shear layers. This was later confirmed when increasing the sound pressure in the duct caused the main acoustic sources in the gap region to shift towards the upstream cylinder. When the four cylinders were considered equivalent to two pairs of two tandem cylinders it was seen that the structure of the propagating vortices were anti-symmetric between each cylinder pair and that the vortices shed between the upstream and downstream cylinder of either pair were in phase with each other. This resulted in an effective mirroring of the net acoustic sources generated over the entire wave cycle for all of the tested cases. Net acoustic sources existed in the shear layer gap region for all the tested cases and it appeared that energy will be generated and absorbed periodically downstream in the wake.

This indicated that the aeroacoustic resonance of the tested cases within the field of view was triggered by a combination of shear layer instability and vortex shedding in the wake, which is similar to that observed for pre-coincidence acoustic resonance of two tandem cylinders.

ACKNOWLEDGMENT

The authors acknowledge funding from the Irish Research Council for Science, Engineering and Technology (IRCSET).

REFERENCES

[1] Blevins, R. D., and Bressler, M. M., 1993. "Experiments on acoustic-resonance in heat-exchanger tube bundles". *Journal of Sound and Vibration,* **164**(3), pp. 503–533.

[2] Ziada, S., Oengoren, A., and Buhlmann, E. T., 1989. "On acoustical resonance in tube arrays part ii: Damping criteria". *Journal of Fluids and Structures,* **3**(3), pp. 315–324.

[3] Fitzpatrick, J. A., 1985. "The prediction of flow-induced noise in heat exchanger tube arrays". *Journal of Sound and Vibration,* **99**(3), pp. 425–435.

[4] Parker, R., 1978. "Acoustic resonances in passages containing banks of heat exchanger tubes". *Journal of Sound and Vibration,* **57**(2), pp. 245–260.

[5] Eisinger, F. L., and Sullivan, R. E., 2007. "Acoustic resonance in a package boiler and its solution - a case study". *Journal of Pressure Vessel Technology,* **129**, pp. 759–762.

[6] Lam, K., Gong, W. Q., and So, R. M. C., 2008. "Numerical simulation of cross-flow around four cylinders in an in-line square configuration". *Journal of Fluids and Structures,* **24**(1), pp. 34–57.

[7] Farrant, T., Tan, M., and Price, W. G., 2000. "A cell boundary element method applied to laminar vortex-shedding from arrays of cylinders in various arrangements". *Journal of Fluids and Structures,* **14**(3), pp. 375–402.

[8] Lam, K., and Lo, S. C., 1992. "A visualization study of cross-flow around four cylinders in a square configuration". *Journal of Fluids and Structures,* **6**(1), pp. 109–131.

[9] Lam, K., and Fang, X., 1995. "The effect of interference of four equispaced cylinders in cross flow on pressure and force coefficients". *Journal of Fluids and Structures,* **9**(2), pp. 195–214.

[10] Finnegan, S. L., Meskell, C., and Ziada, S., 2009. "Experimental investigation of the aeroacoustic sources in a tandem cylinder configuration". In 2009 ASME Pressure Vessels and Piping Division Conference.

[11] Finnegan, S. L., Meskell, C., and Ziada, S., (Under Review). "Experimental investigation of the acoustic power around two tandem cylinders.". *Journal of Pressure Vessel Technology*.

[12] Howe, M. S., 1975. "Contributions to theory of aerodynamic sound, with application to excess jet noise and theory of flute". *Journal of Fluid Mechanics*, **71**(4), pp. 625–673.

[13] Howe, M. S., 1980. "The dissipation of sound at an edge". *Journal of Sound and Vibration,* **70**(3), pp. 407–411.

[14] Zdravkovich, M. M., 1985. "Flow induced oscillations of two interfering circular cylinders". *Journal of Sound and Vibration,* **101**(4), pp. 511–521.

[15] Mohany, A., and Ziada, S., 2005. "Flow-excited acoustic resonance of two tandem cylinders in cross-flow". *Journal of Fluids and Structures,* **21**(1), pp. 103–119.

[16] Oengren, A., and Ziada, S., 1992. "Vorticity shedding and acoustic resonance in an in-line tube bundle part ii: Acoustic resonance". *Journal of Fluids and Structures,* **6**(3), pp. 293–302.

[17] Hourigan, K., Welsh, M. C., Thompson, M. C., and Stokes, A. N., 1990. "Aerodynamic sources of acoustic resonance in a duct with baffles". *Journal of Fluids and Structures,* **4**(4), pp. 345–370.

[18] Parker, R., 1967. "Resonance effects in wake shedding from parallel plates: Calculation of resonant frequencies". *Journal of Sound and Vibration,* **5**(2), pp. 330–343.

[19] Lighthill, M. J., 1952. "On sound generated aerodynamically. i. general theory". *Proceedings of the Royal Society of London. Series A, Mathematical and Physical Sciences,* **211**(1107), pp. 564–587.

[20] Velikorodny, A., Yan, T., and Oshkai, P., 2010. "Quantitative imaging of acoustically coupled flows over symmetrically located side branches". *Experiments in Fluids,* **48**(2), pp. 245–263.

[21] Rockwell, D., and Naudascher, E., 1978. "Review - self-sustaining oscillations of flow past cavities". *Journal of Fluids Engineering-Transactions of the ASME,* **100**(2), pp. 152–165.

[22] Finnegan, S. L., Meskell, C., and Ziada, S., 2010. "The effect of sound pressure on the aeroacoustic sources around two ducted tandem cylinders". In ASME 2010 3rd Joint US-European Fluids Engineering Summer Meeting and 8th International Conference on Nanochannels, Microchannels, and Minichannels.

[23] Mohany, A., and Ziada, S., 2009. "Numerical simulation of the flow-sound interaction mechanisms of a sinlge and two-tandem cylinders in cross-flow". *Journal of Pressure Vessel Technology,* **131**(3).